Mohammadi, N., Sodoudi, F., Mohammadi, E., Sadidkhouy, A. (2013): New constraints on lithospheric thickness of the Iranian plateau using converted waves. - Journal of Seismology, 17, 3, 883-895

DOI: 10.1007/s10950-013-9359-2

New constraints on lithospheric thickness of the Iranian Plateau using converted waves

Najmieh Mohammadi[1], Forough Sodoudi[2,3], Elham Mohammadi[1], Ahmad Sadidkhouy[1]

[1] Institute of Geophysics, University of Tehran, 14155-6466, Tehran, Iran

[2] Helmholtz Centre Potsdam, GFZ German Research Centre for Geosciences, Telegrafenberg, 14473 Potsdam, Germany

[3] Freie Universität Berlin, Malteserstr. 74-100, 12249 Berlin, Germany

email: nmohammadi@ut.ac.ir

Abstract

Study of mantle lithosphere plays a key role to reveal predominant tectonic setting process of a region. The current geological and tectonic setting of Iran is due to the ongoing continental–continental collision of Arabian and Eurasian plates. We applied a combined P and S receiver function analysis to the teleseimic data of 9 permanent broadband seismic stations of the International Institute of Earthquake Engineering and Seismology (IIEES) located in different tectonic zones of Iranian plateau. More than 4 years of data were used to estimate the thickness of the crust and mantle lithosphere. According to our results, the crust is 50 km thick beneath the Zagros Fold and Thrust Belt (ZFTB). We found the maximum Moho depth of approximately 70 km under the Sanandaj-Sirjan zone (SSZ) indicating the overthrusting of the crust of Central Iran onto the Zagros crust along the Main Zagros Thrust (MZT). Below the northeasternmost part of the Urumieh–Dokhtar Magmatic Arc (UDMA) and Central Iran, the Moho becomes shallower and lies at 40 km depth. Towards northeast, beneath the Alborz zone, the crust is 55 km thick. Based on S receiver functions, we provided new insights into the thickness of the Arabian and Eurasian lithospheres. The location of the boundary between these plates was estimated to be beneath the SSZ, which is slightly shifted northeastward relative to the surficial expression of the MZT. Furthermore, the Arabian plate is characterized by the relatively thick lithosphere of about 130 km beneath the ZFTB reaching 150 km beneath the SSZ, where the thickest crust was also observed. This may imply that the shortening across the Zagros is accommodated by lithospheric thickening. In contrast, the UDMA and Central Iran are recognized by the thin lithosphere of about 80-85 km. This thin lithosphere may be associated with the asthenospheric upwelling caused by either lithospheric delamination or Neo-Tethys slab detachement beneath the Zagros collision zone.

Key words: S receiver function, P receiver function, Moho, Lithosphere - Asthenosphere Boundary, Iranian plateau, collision zone

1. Introduction

The current tectonics of the Iranian plateau resulted from the collision of the Arabian and Eurasian Plates in the early Miocene, which is due to the subduction of the Neo-Tethys oceanic plate beneath Eurasia plate (Sengor and Yilmaz 1981; Jackson and McKenzie 1984; Dewey et al. 1986). Estimates on the age of collision between Arabia and Eurasia range from late Cretaceous to Pliocene, based on a wide variety of presumed geologic responses (Berberian and King 1981; Allen et al., 2004). This convergence has made different seismotectonic zones with various geological formations within Iranian plateau (Fig. 1). The Zagros Fold and Thrust Belt (ZFTB) as an active tectonic structure has been formed during collision of Arabian and Central Iranian plates along the Main Zagros Thrust (MZT), which is believed to have been the active thrust fault between Arabia and Iran during subduction (Falcon 1974)(see Fig. 1). According to GPS data (Vernant et al. 2004), the N–NE convergence of the Arabian plate towards Eurasia is estimated about 22±2 mm/year, which results in crustal shortening and thickening in ZFTB zone (Jackson et al. 1995). The MZT separates ZFTB from the Sanandaj-Sirjan zone (SSZ). Geological evidence including ophiolitic sequence along MZT (Molinaro et al. 2005) and calc alkaline magmatic volcanism (Agard et al. 2005) implies that the SSZ experienced various metamorphic episodes during the subduction of the Tethyan Ocean under the Iranian microplate. During the latest metamorphic episode, the SSZ overthrusted the Zagros sedimentary sequence along the MZT (Stöcklin 1968; Agard et al. 2005). Parallel to SSZ is the Urumieh–Dokhtar magmatic arc (UDMA), which consists of Andean-type, subduction-related volcanic arc. This zone is known for continues volcanic activity from Eocene to present (Berberian and King 1981). Central Iran is an intraplate environment located between two geosutures of paleotethys (Kopeh Dagh in northeast of Iran) and Neotethys (Zagros in southwest of Iran). Rifting within Arabian-Iranian platform during the late Paleozoic is assumed to cause the advent of the Neotethys Ocean and the separation between these plates at the Main Zagros Thrust (Berberian 1983). The northward convergence of the Central Iran micro continent and the northwestward displacement of the South Caspian Basin with respect to Eurasia resulted in forming the Alborz Mountains limited to an active, arcuate fold-and-thrus belt with high seismicity (Jackson and McKenzie 1984). Based on GPS measurments, Alborz undertakes a N–S shortening about 5 ± 2 mm/year across the Central Alborz (Vernant et al. 2004).

The boundary between the lithosphere and asthenosphere is a fundamental boundary in the plate tectonics separating the rigid outer shell of the earth from the ductile convecting materials below. Investigation of the earth's lithosphere, particularly the Lithosphere-Asthenosphere Boundary (LAB) is a very important topic with great

scientific sense related to global dynamics of the earth and can provide new insights into a better understanding of the mechanism of formation and history of deformation of the Iranian plateau. Studies focused on the nature and depth of the LAB beneath Iranian plateau are rare (e.g., Taghizadeh-Farahmand et al., 2010; Sodoudi et al., 2009), whereas significant constraints on the nature of the crustal structure beneath different tectonic zones of Iran have been provided yet.

The gravity map of Iranian plateau prepared by Dehghani and Makris (1984) revealed a crustal thickness of about 55 km beneath ZFTB. They also found a thinner crust of 35 km beneath the Alborz mountains. Snyder and Barazangi (1986) estimated a Moho depth of about 65 km under ZFTB based on gravity observations. Paul et al. (2006) installed a profile across the Zagros belt and analyzed P receiver functions to determine the Moho depth. They found the maximum Moho depth of about 70 km beneath the Sanandaj-Sirjan Zone decreasing to about 42 km under UDMA and Central Iran. They interpreted this abrupt crustal thickening beneath SSZ as the result of underthrusting the crust of Zagros beneath Central Iran along the MZT. Afsari et al. (2011) estimated the lateral variation of the Moho boundary beneath the Northwest Zagros and Central Iran using P receiver functions. They found a relatively flat Moho of about 42 km beneath the Northwest Zagros and Central Iran deepening toward the Sanandaj-Sirjan Metamorphic Zone and reaches 51 km, where two crusts (Zagros and Central Iran) are assumed to be superposed. They also showed that the Moho depth decreases toward the Urmieh-Dokhtar Cenozoic volcanic belt and reaches 43 km.

A seismic technique based on converted waves (P-to-S, e.g., Vinnik, 1977, and S-to-P, Farra and Vinnik, 2000) has now been developed far enough to detect the LAB with a high resolution (e.g., Abt et al., 2010; Geissler et al., 2010; Heit et al., 2007; Kawakatsu et al., 2009; Kumar et al., 2006, 2007; Oreshin et al., 2002; Rychert and Shearer, 2009; Sodoudi et al., 2006a, 2006b, 2009, 2011; Yuan et al., 2006; Vinnik et al., 2004). Based on S receiver function analysis, Sodoudi et al. (2009) presented a relatively thin lithosphere of 90 km beneath the high Central Alborz zone. McKenzie and Priestley (2007) estimated a thick lithosphere of about 260 km beneath Iran using low-resolution surface waves and suggested that the process that generated the thickened crust beneath Iranian plateau has also resulted in thick lithosphere that extends beneath the whole plateau. Teleseismic P wave tomography and Rayleigh wave dispersion measurements (Kaviani et al. 2007) as well as teleseismic tomography based on S phase inversion (Keshvari et al. 2011) revealed a low velocity zone at ~80 km beneath Central Iran and UDMA. Furthermore, a combined study including gravity, geoid, and topography data by Molinaro et al. (2005) showed that the lithospheric thickness decreases from 200 km beneath the Arabian platform to about 100 km beneath the UDMA. More recently, Shad Manaman et al. (2010) used the Partitioned Waveform Inversion (PWI) method and showed that the relatively old and cold Arabian plate has higher velocity at depth than the younger lithosphere of Central Iran. They found also a sharp and steep subcrustal boundary roughly coincident with the surficial expression of the MZT, separating two different mantle domains.

The main objective of this paper is to image the topography of the Moho and the LAB beneath different tectonic zones of Iranian plateau including Zagros, Alborz and Central Iran using P and S receiver functions.

2. Data and method

We used data from 9 permanent broadband seismic stations of the International Institute of Earthquake Engineering and Seismology (IIEES) located in the different geological zones of Iran (Fig. 2). Table 1 shows the geographical coordinates of the seismic stations. All stations are equipped with Güralp CMG3T seismometers. More than 4 years of data (2006-2010) were used for P and S receiver function analysis. We utilized 100 events with magnitude greater than 5.5 (Mb) at epicentral distances between 30° and 90° for P receiver function analysis (Fig. 3). 76 teleseismic events with clear S onset at epicentral distances between 60°-85° with magnitude larger than 5.7 (Mb) were used for S receiver function calculation (Fig. 3). These epicentral distances were suggested by Faber and Müller (1980) as the best distance to detect the converted S-to-P phases from the Moho and LAB. The methodologies (P and S receiver function) used in this paper are the same as those described by Yuan et al. (1997) and Kumar et al. (2005a, 2005b), respectively. We rotate the ZNE-component waveforms into the local LQT ray-based coordinate system and deconvolve the L component from the Q component to isolate the P-to-S conversions on the Q component for P receiver function calculation.

S receiver function method is based on the detection of time difference in arrival of the S-to-P phase related to the direct S wave from discontinuities underneath a seismic station and calculation the depth using a reference velocity model (Farra and Vinnik 2000). S receiver functions (SRFs) are noisier than P receiver functions (PRFs) due to their later arrivals than direct P wave. Furthermore, they contain longer periods compared to the PRFs, therefore thin contrast velocity discontinuities in the crust and upper mantle can not be resolved by SRFs. However, S receiver functions are not influenced by multiples because the converted S-to-P phases arrive earlier than the direct S wave. This advantage enables SRF to detect the LAB with higher resolution than PRF. For S receiver function calculation we considered a time window of 200 seconds (100s before the S onset) and eliminated the instrument response. Rotation under incidence angle should be precisely performed. The best incidence angle is defined by the minimum of energy in the L component at arrival time of the direct S phase (see Kumar et al., 2006). To remove the source and ray path effects, S waveforms on the Q component were deconvolved from the corresponding L and T components. As expected, the L components contain the converted S-to-P phases. The polarity of the S receiver function reversely appears due to the different sign of the S-to-P conversion coefficients compared with the PRF. Therefore we reversed the amplitudes as well as the time axis of the SRF. We applied a low-pass filter of 1s and 4s to the P and SRF data, respectively. Then they are move-out corrected to the reference slowness of 6.4 s/deg. This slowness is not necessarily realistic for S waves, but it is used to make P and S receiver function time scales directly comparable.

The times in the P and SRF traces can be also converted into the depth domain using the reference velocity model (in this study IASP91 model, Kennett and Engdahl, 1991). If we assume that the seismic velocity varies in the crust by up to 5%, this procedure may introduce an error of 3 km in the Moho depth and 5 km in the LAB

depth. Regarding dominant wave periods of the P and S waves and additional errors produced by lateral heterogeneities or/and noise, we roughly estimate the errors in the depth determination to be less than 5 km (using P receiver functions), and about 10 km using S receiver functions.

3. Observations

We computed PRFs for all stations. Individual and summed PRFs for stations THKV and SNGE are presented in Fig 4. They are sorted by the back azimuth. Beneath the station THKV located in the central Alborz zone, the primary converted phase from the Moho arrives at a delay time of approximately 6.5 s. This phase is seen at 5 s beneath the station SNGE located in SSZ. Due to the different tectonic settings exist in the study area, we divided the whole region into 4 main zones. These zones include Alborz, Urumieh-Dokhtar Magmatic Arc (UDMA), Sanandaj-Sirjan Zone (SSZ) and Zagros Fold and Thrust Belt (ZFTB) (see Figs. 1&2). We summarized our results in Figure 5. For each zone, PRFs are stacked in bins of 0.05° and sorted by the latitude of their piercing points at 50 km depth (approximate Moho depth, see Fig. 2). The obtained crustal structures seem to be complicated and there are also some evidences for anisotropy/dipping (reversal of polarity) effects. However, these topics are beyond the scope of this paper and we just concentrate on the crustal thickness based on the arrival times of the P-to-S converted phases. As Fig. 5 shows PRFs provided a clear image of the Moho boundary beneath each tectonic zone (shown with red dashed lines). The converted Moho phase is observed at times ranging between 5-8 s. The largest arrival time is seen beneath the SSZ zone (~8s).

S receiver functions were also calculated for each station and tectonic zone (Fig. 6). Due to the wide distribution of the S-to-P conversion points compared to those of P-to-S waves, the estimated delay times of the converted S-to-P waves can not be directly attributed to the seismic discontinuities beneath the station (see Fig. 2). We calculated here the distribution of the S-to-P piercing points at 100 km depth (approximate depth of the continental LAB). As Fig. 2 shows, the S-to-P converted waves sample the areas, where are poorly covered by the P-to-S converted waves. Therefore, SRFs can additionally obtain information about the deeper structure beneath the Central Domain (CD) and Central Iranian Plateau (CIP). We sorted the SRFs in each tectonic zone by the latitude of their piercing points at 100 km depth and showed them beneath the Alborz and ZFTB regions in Fig. 6. Two phases are visible in the SRF data. The first phase (in black) indicates the Moho boundary, while the second stable and coherent phase (in gray) most probably stem from the LAB (labeled L). The LAB converted phase seems to be much deeper beneath the ZFTB (~13s) compared to that observed beneath the Alborz tectonic zone (~10s).

4. Discussion

We converted delay times of the Moho conversions into the depth domain using the reference velocity model of IASP91 and show them along a SW-NE trending profile crossing all tectonic zones (see Fig. 2). The values are also listed in Table 2. The correlation obtained between our P and S receiver functions is significant (Fig. 7). The Moho phases, which are reliably resolved by the PRF data (Fig. 7, upper panel), can be also clearly observed in the SRF data (Fig. 7, lower panel). The small time differences between the estimated P-to-S and S-to-P converted phases at the Moho boundary can be caused by the longer period content of the S receiver functions as well as their differing piercing points compared to those of the P receiver functions (see Fig. 2). However, the differences are within the expected uncertainties (~5 km). Based on our results, we found the thickest crust of approximately 70 km beneath the SSZ, whereas the thinnest crust (~37-40 km) was seen beneath the CIP and CD, where the topography is lowest (Fig. 7).

Beneath the Alborz zone, the crust is 55 km thick under the high elevations of Alborz (Figs. 5a & 7). These results are in good agreement with those obtained by Sodoudi et al. (2009) in Central Alborz using P and S receiver functions of short period stations and can be also confirmed by the results of simultaneous inversion of receiver functions and fundamental mode of Rayleigh wave group velocity done by Radjaee et al. (2010). Our PRFs also revealed a local crustal thickening to about 67 km beneath the DMV station (see Fig. 5a, middle part), which was previously reported by Sodoudi et al (2009) under the Damavand volcano. The Moho depths obtained for the CD and CIP come mainly from our SRF analysis (see Fig. 2). We found a relatively flat Moho at 37 and 40 km depth beneath the CD and CIP, respectively (Fig. 7). These results are supported by those derived by Paul et el. (2006, 2010) and Afsari et al. (2011) using P receiver functions. Beneath the ZFTB, the crust is 50 km thick (Fig.s 5b & 6b). This result is in a good agreement with that showed along the Zagros01 & Zargos03 profiles by PRFs (Paul et al., 2006, 2010). The average Moho depth along the Zagros collisional zone was also estimated to be about 40–45 km using the partitioned waveform inversion (PWI) method (Shad Manaman et al., 2010).

Based on PRFs, the crust seems to have different thicknesses beneath the UDMA zone (Fig. 5c). For the stations located within the UDMA zone, the crust is 50-60 km thick. Towards northeast in the boundary with the CD zone, the crust shallows to a depth of about 40 km (see also Fig. 2). This depth correlates well with that obtained from our SRFs beneath the CD zone (see Fig. 7) and is compatible with those derived from previous studies (Paul et al. 2006, Afsari et al. 2011, Shad Manaman et al. 2011). SRFs showed the Moho at 50 km depth beneath the UDMA (see Fig. 7). However, regarding their piercing points they mostly sample the northwestern part of the UDMA zone (see Fig. 2).

The thickest crust was seen beneath the SSZ (Fig. 5d). We found an average crustal thickness of about 40 km beneath the northwestern part of the SSZ, whereas an abrupt crustal thickening up to about 70 km was clearly shown beneath the central part of the SSZ by our PRFs. Despite the small number of the SRFs, they also imaged a thick crust of about 60 km beneath the SSZ (Fig. 7). These results are in good correlation with those provided by the previous works in Zagros (Paul et al., 2006, 2010; Shad Manaman et al., 2010). Paul et al. (2006, 2010) proposed that localized thickening

beneath the SSZ is resulted from the overthrusting of the crust of Central Iran on the Zagros crust along the MZT.

To summarize our results we presented in Fig. 8 the stacked SRFs obtained from different tectonic zones along the SW-NE trending profile (see Fig. 2). The arrival time of the LAB phase varies between 9 and 15 s. We found the largest arrival time (~15 s) beneath the SSZ, whereas the smallest arrival time of about 9 s is observed beneath the CD tectonic zone.

According to our SRF section, the lithosphere is estimated to be 130 km thick beneath the ZFTB, which thickens to about 150 km underneath the SSZ (Fig. 8). Towards northeast, beneath the UDMA zone the LAB is relatively shallow and lies at 85 km depth. We observed the thinnest lithosphere of about 80 km beneath the CD zone. The lithosphere seems to be about 90 km thick under the Alborz zone. Based on results the thickest lithosphere (~150 km) is located beneath the SSZ, where the thickest crust is also observed (~70 km) (see Fig. 7).

The negative velocity anomaly characterizing the upper mantle of Iran north of the MZT has been widely documented (e.g. Debayle et al. 2001; Kaviani et al. 2007; Maggi & Priestley 2005; Shapiro & Ritzwoller 2002; Shad Manaman & Shomali 2010). However, its continuation southward is still under debate (Paul et al. 2006; Kaviani et al. 2007). Kaviani et al. (2007) documented a strong lateral change of both P- and S-wave velocities in the shallow mantle beneath the Central Zagros using surface wave dispersion data. They estimated an increase of the S-wave velocity from 4.5 km/s at Moho depth (45 km) to about 4.9 km/s at 250 km depth beneath the ZFTB with no detectable LVZ suggesting that the thickness of the lithosphere is at least 250 km under the ZFTB. Even though they found a LVZ at 80 km depth beneath the suture region from the MZT to the UDMA.

High resolution tomography images provided by Shomali et al. (2011) revealed a thick continental lithosphere (more than 200 km) beneath the Arabian shield (ZFTB) and no (or very thin) lithospheric mantle under the Central Iran. Furthermore, they indicated that the low-velocity anomaly beneath UDMA continues with less intensity underneath the ZFTB to depths of about 200 km. However due to the limited resolution of the data, they could not precisely estimate the positions of these small anomalies. Shad Manaman et al. (2010) obtained new seismic velocity models based on surface wave tomography. They showed a sharp lithospheric transition at the MZT between 150 and 400 km depth with higher S-velocity (~2–3%) within the Arabian lithosphere compared with that in the lithosphere of the Central Iran. They found also a relatively low velocity layer between depth intervals of order of 80–150 km along the Central Zagros, which was interpreted as an indication of lithospheric delamination within the Arabian lithosphere. However, these results are in contrast with those previously reported by Mckenzie and Priestley (2007) suggesting a thick lithosphere of 260 km beneath Iranian Plateau with no large scale lithospheric removal at any time since the formation of the plateau.

A large number of geological and geophysical studies (e.g., Carminati et al., 1998; Davies and von Blanckenburg, 1995; Wong A Ton and Wortel, 1997; Wortel and Spakman, 2000; van de Zedde and Wortel, 2001) indicate that continental-continental collision can lead to the slab detachment and subsequent slab sinking into the mantle,

which allows mantle upwelling materials to subcrustal layers. Furthermore, there are different evidences for the volcanic activities in UDMA and SSZ (e.g., Molinaro et al., 2005). However, there is still some uncertainty related to the evolution of the oceanic slab which subducted before continental collision due to the lack of deep seismicity under the Zagros region and the absence of high velocity anomaly related to the oceanic slab beneath the UDMA and Central Iran.

SRFs enabled us to produce the first clear image of the base of the lithosphere beneath the Zagros collision zone and its continuation northward (Fig. 8). Presence of two different lithospheres can be well seen along our SW-NE profile. On the other hand, an increase in lithospheric thickness across the Zagros collision zone is assumed to separate two different lithospheres namely the Arabian (to the southwest) and the Central Iranian (to the northeast) domains. We interpret the LAB at 130 km depth beneath the ZFTB, which deepens to about 150 km beneath the SSZ as the Arabian LAB. Whereas the relatively shallow LAB of about 80-85 km beneath the northeasternmost part of the UDMA and CD is interpreted as the Central Iranian LAB. Thus, it seems that the abrupt thickening of the crust and lithosphere is occurred beneath the SSZ (up to 70 and 150 km, respectively). This may imply that the strongest thickening is slightly shifted to the NE relative to the highest topography in good agreement with Paul et al. (2006) and Shad Manaman et al. (2010). We interpret the significantly depressed Moho (70 km) (Fig. 7) and the thick lithosphere (150 km) under the SSZ (Fig. 8) as the results of the horizontally shortening and vertically thickening of the Arabian lithosphere due to the collision with the Central Iranian Plate. It may suggest that the stress caused by the continental collision has influenced the whole Arabian lithosphere beneath the SSZ. Furthermore, we estimate the location of the boundary between the two lithospheres beneath the northernmost part of the SSZ showing that the Arabian lithosphere extends at least to northeast of the surface trace of the MZT. This finding is more accurate rather than the previous results obtained from long period surface waves indicating a lithospheric boundary between 100 km and 250 km depth beneath the MZT.

Furthermore, a thickness of 130 km seems realistic for the Arabian lithosphere and correlates well with those obtained from various geophysical studies, which mostly estimated a thickness between 100 and 160 km for the Arabian lithosphere (Stern & Johnson, 2010). This value is also close to the thermal lithospheric thickness estimates expected by Artemieva and Mooney (2001) for the Arabian plate. However, this thickness can not be considered as a reliable factor to control the high elevations of Zagros, which are also not underlain by the thickest crust (~ 50 km). We suggest in good agreement with Shomali et al. (2011) that the high elevation in the ZFTB is supported by hot and shallow asthenosphere rather than a thickened crust and lithosphere. The same scenario was previously reported beneath the high Alborz mountain (Sodoudi et al., 2009). A relatively thin lithosphere of about 90 km beneath the Alborz zone may also imply that the high central Alborz mountain range is being thermally supported by asthenospheric material. The high Alborz topography may be also explained by the underthrusting of the oceanic crust of the South Caspian Basin from north (Priestley et al. 1994; Axen et al. 2001; Jackson et al. 2002; Tatar et al. 2007) and the underthrusting of the Central Iranian plateau from south (McKenzie 1972; Jackson and McKenzie 1984; Priestley et al. 1994) beneath the Alborz mountains.

Our observations as well as the sudden change in the LAB depth along our profile under the Zagros suture zone (SSZ) may support the idea that the subducted Neo-Tethys oceanic slab has broken-off under the region of maximum Moho depth (SSZ). Bird (1978) used finite element modeling and showed that the slab detachment can cause a gap at depth between the lithospheres of Arabia and Eurasia under the MZT. The shallow LAB observed beneath the northernmost UDMA and Central Iran is most likely originated by active upwelling of the asthenospheric material into shallower mantle due to slab break-off and sinking into the mantle (Molinaro et al., 2005a; Shad Manaman et al., 2010; Shomali et al., 2011). Another explanation for the observed LAB thickness estimates points to lithospheric delamination underneath the SSZ (Shad Manaman et al., 2011). Shortening and thickening of the Arabian lithosphere associated with the collision process beneath the SSZ may result in the delamination of the lower part of Arabian lithosphere and subsequently upward flowing of the asthenospheric material into the shear zone (depth 80-85 km beneath UDMA and CD). Finally, we conclude that asthenospheric upwelling caused by either delamination or slab detachment played the main role in formation of the thin lithosphere beneath the Central Iran.

5. Conclusion

P and S receiver functions obtained from teleseismic events recorded at nine broadband stations of the IIEES have been used to determine the variations of the crustal and lithospheric thickness across a SW-NE profile from Zagros collision zone to the high Alborz elevations. The crust was estimated to be 50 km thick beneath the ZFTB. However, we clearly observed a significant crustal thickening to a depth of 70 km beneath the SSZ, where the crust of Central Iran is assumed to overthrust the crust of the Zagros along the MZT. Towards northeast, the crust starts to thin and becomes 40 km beneath the Central Iran, where the topography is lowest. Beneath the Central Alborz the crustal thickness is estimated to be 55 km. S receiver functions enabled us to resolve a clear image of the collision between the Arabian and Eurasian lithospheres. We estimated the location of the boundary separating the two lithospheres beneath the SSZ, which is not coincident with the surficial expression of the MZT. Furthermore, we observed a relatively thicker lithosphere of about 130 km for the Arabian plate beneath ZFTB compared to that of 80-85 km recognized beneath the northeasternmost part of the UDMA and Central Iran. The thickest lithosphere (150 km) was imaged beneath the SSZ, where the thickest crust was also found. This may imply that the whole lithosphere beneath SSZ has been affected by the continental collision. Even though, the presence of the thin lithosphere below the UDMA and Central Iran would support the asthenospheric upwelling to subcrustal levels due to either lithospheric delamination or slab detachment beneath the Zagros collision zone.

Acknowledgements

Authors are thankful to the International Institute of Earthquake Engineering and Seismology (IIEES) for providing the teleseismic waveforms. We used the software packages SeismicHandler (Stammler 1993) for data processing and GMT (Wessels and Smith 1998) for plotting. We would like to thank Torsten Dahm and two anonymous reviewers for their helpful suggestions that greatly improved this paper.

References

Abt DL, Fischer KM, French SW, Ford HA, Yuan H, Romanowicz B (2010) North American lithospheric discontinuity structure imaged by Ps and Sp receiver functions. J Geophys Res 115: B09301

Agard P, Omrani J, Jolivet L, Mouthereau F (2005) Convergence history across Zagros (Iran): constraints from collisional and earlier deformation. Int J Earth Sci 94:401-419

Afsari N, Sodoudi F, Taghizadeh Farahmand F, Ghassemi MR (2011) Crustal structure of Northwest Zagros (Kermanshah) and Central Iran (Yazd and Isfahan) using teleseismic Ps converted phases. J Seismol 15:341-353

Allen MB, Jackson J, Walker R (2004) Late Cenozoic reorganization of the Arabia-Eurasian collision and the comparison of short-term and long-term deformation rates. Tectonics 23:TC2008

Artemieva IM, Mooney WD (2001) Thermal thickness and evolution of Precambrian lithosphere: a global study. J Geophys Res B106: 16387-16414

Axen GJ, Lam PS, Grove M, Stockli DF (2001) Exhumation of the west-central Alborz Mountains, Iran, Caspian subsidence, and collision-related tectonics. Geology 29: 559–562

Berberian M, King GCP (1981) Towards a paleogeography and tectonic evolution of Iran. Can J Earth Sci 18:210-265

Berberian M (1983) The southern Caspian: A compression depression floored by a trapped modified oceanic crust. Can J Earth Sci 20 (2): 163-183

Bird P (1978) Finite element modeling of lithosphere deformation: the Zagros collision orogeny. Tectonophysics 50:307-336

Carminati E, Wortel MJR, Spakman W, Sabadini R (1998) The role of slab detachment processes in the opening of the western-central Mediterranean basins: some geological geophysical evidence. Earth Planet Sci Lett 160: 651-665

Davies JH, von Blanckenburg F (1995) Slab breakoff: a model of lithosphere detachment and its test in the magmatism and deformation of collisional orogens. Earth Planet Sci Lett 129: 85-102

Debayle E, Leveque JJ, Cara M (2001) Seismic evidence for a deeply rooted low-velocity anomaly in the upper mantle beneath the northeastern Afro-Arabian continent. Earth Planet Sci Lett 193(3-4): 423-436

Dehghani GA, Makris J (1984) The gravity field and crustal structure of Iran. Neues Jahrbuch Geol. Palaeont. Abh 168:215-229

Dewey JF, Hempton MR, Kidd WSF, Saroglu F, Sengor AMC (1986) Shortening of continental lithosphere: the neotectonics of eastern Anatolia-a young collision zone, In: Coward M,P, Ries A,C, (Eds,) Collision Tectonics. Geol Soc London pp:3-36

Faber S, Müller G (1980) Sp phases from the transition zone between the upper and lower mantle. Bull Seismol Soc Am 70:487-508

Falcon NL (1974) Southern Iran: Zagros mountains. Spec Pub Geol Soc Lond 4:199-211

Farra V, Vinnik L (2000) Upper mantle stratification by P and S receiver functions. Geophys J Int 141:699-712

Geissler WH, Sodoudi F, Kind R (2010) Thickness of the central and eastern European lithosphere as seen by S receiver functions. Geophys J Int 181(2): 604-634. doi: 10.1111/j.1365-246X.2010.04548.x

Heit B, Sodoudi F, Yuan X, Bianchi M, Kind R (2007) An S-receiver function analysis of the lithospheric structure in South America. Geophys Res Lett 34:L14307.

Jackson J, McKenzie D (1984) The active tectonics of the Alpine-Himalayan belt between western Turkey and Pakistan. Geophys J R astr Soc 77:185-264

Jackson J, Hains J, Holt W (1995) The accommodation of Arabia-Eurasia plate. J Geophys Res 100:15205- 15219

Jackson J, Priestley K, Allen M, Berberian M (2002) Active tectonics of the South Caspian Basin. Geophys J Int 148(2):214-245

Kawakatsu H, Kumar P, Takei Y, Shinohara M, Kanazawa T, Araki E, Suyehiro K (2009) Seismic evidence for sharp lithosphere-asthenosphere boundaries of oceanic plates. Science 324: 499-502

Kaviani A, Paul A, Bourova E, Hatzfeld D, Pedersen H, Mokhtari M (2007) A strong seismic velocity contrast in the shallow mantle across the Zagros collision zone (Iran). Geophys J Int 171:399-410

Keshvari F, Shomali ZH, Tatar M, Kaviani (2011) A Upper-mantle S-velocity structure across the Zagros collision zone resolved by nonlinear teleseismic tomography. J Seismol 15:329-339

Kennett BLN, Engdahl ER (1991) Travel times for global earthquake location and phase identification. Geophys J Int 105: 429-465.

Kumar P, Kind R, Hanka W, Wylegalla K, Reigber Ch, Yuan X, Woelbern I, chwintzer P, Fleming K, Dahl-Jensen T, Larsen TB, Schweitzer J, Priestley K, Gudmundsson O, Wolf D (2005a) The lithosphere-asthenosphere boundary in the North-West Atlantic region. Earth Planet Sci Lett 236:249-257

Kumar P, Kind R, Kosarev G (2005b) The lithosphere-asthenosphere boundary in the Tien Shan-Karakoram region from S receiver functions: evidence for continental subduction. Geophys Res Lett 32:L07305

Kumar P, Yuan X, Kind R, Ni J (2006) Imaging the colliding Indian and Asian continental lithospheric plates beneath Tibet. J Geophsy Res 111:B06308. doi:10.1029/2005JB003930

Kumar P, Yuan X, Kumar MR, Kind R, Li X, Chadha RK (2007) The rapid drift of the Indian tectonic plate. Nature 449:894–897. doi:10.1038/nature06214

Maggi A, Priestley K (2005) Surface waveform tomography of the Turkish-Iranian plateau. Geophys J Int 160: 1068-1080

McKenzie D (1972) Active tectonics of the Mediterranean region. Geophys J R Astr Soc 30:109-185. doi: 10.1111/j.1365-246X.1972.tb02351.x

McKenzie D, Priestley K (2007) The influence of lithospheric thickness variations on continental evolution. Lithos 102:1-11

Molinaro M, Zeyen H, Laurencin X (2005a) Lithospheric structure beneath the south-eastern Zagros Mountains, Iran: recent slab break-off?. TerraNova 17:1-6

Oreshin S, Vinnik L, Peregudov D , Roecker S (2002) Lithosphere and asthenosphere of the Tien Shan imaged by S receiver functions. Geophys. Res. Lett 10.1029/2001GL014441

Paul A, Kaviani A, Hatzfeld D, Vegne J, Mokhtari M (2006) Seismological evidence for crustal- scale thrusting in the Zagros mountain belt (Iran). Geophys J Int 166:227-237

Paul A, Hatzfeld D, Kaviani A, Tatar M, Pequegnat C (2010) Seismic imaging of the lithospheric structure of the Zagros mountain belt (Iran). Geol Soc London Special Publications 330:5-18

Priestley K, Baker C, Jackson J (1994) Implications of earthquake focal mechanism data for the active tectonics of the south Caspian basin and surrounding regions. Geophys J Int 118:111-141

Radjaee A, Rham D, Mokhtari M, Tatar M, Priestley K, Hatzfeld D (2010) Variation ofMoho depth in the central part of the Alborz Mountains northern Iran. Geophys J Int 181:173-184

Rychert C, Shearer P (2009) A global view of the lithosphereasthenosphere Boundary. Science 324: 495-498

Sengor AMC, Yilmaz Y (1981) Tethyan evolution of Turkey: a plate tectonic approach. Tectonophysics 75:181-241

Shad Manaman, N, Shomali H (2010) Upper mantle S-velocity structure and Moho depth variations across Zagros belt, Arabian-Eurasian plate boundary. Phys Earth planet Inter 180:92-103

Shad Manaman N, Shomali H, Hemin K (2011) New constraints on upper-mantle S-velocity structure and crustal thickness of the Iranian plateau using partitioned waveform inversion. Geophys J Int 184: 247-267

Shapiro NM, Ritzwoller MH (2002) Monte-Carlo inversion for a global shear-velocity model of the crust and upper mantle. Geophys J Int 151: 88-105.

Sodoudi F, Yuan X, Liu Q, Kind R, Chen J (2006a) Lithospheric thickness beneath the Dabie Shan, central eastern China from S receiver functions. Geophys J Int 166(3):1363-1367

Sodoudi F, Kind R, Priestley W, Hanka W, Wylegalla K, Stavrakakis G, Vafidis A, Harjes HP, Bohnhoff M (2006b) Lithospheric structure of the Aegean obtained from P and S receiver functions. J Geophys Res 111:12307-12330

Sodoudi F, Yuan X, Kind R, Heit B, Sadidkhouy A (2009) Evidence for a missing crustal root and a thin lithosphere beneath the Central Alborz by receiver function studies. Geophys J Int 177(2):733-742

Sodoudi F, Yuan X, Asch G, Kind R (2011) High-resolution image of the geometry and thickness of the subducting Nazca lithosphere beneath northern Chile. J Geophys Res 116: B04302

Shomali ZH, Keshvari F, Hassanzadeh J, Mirzaei N (2011) thospheric structure beneath the Zagros collision zone resolved by non-linear teleseismic tomography. Geophys J Int 187: 394-406

Snyder DB, Barazangi M (1986) Deep crustal structure and flexure of the Arabian plate beneath the Zagros collisional mountain belt as inferred from gravity observations. Tectonics 5:361-373

Stern Rj, Johnson P (2010) Continental lithosphere of the Arabian Plate: A geologic, petrologic, and geophysical synthesis, Earth-Science Reviews 101: 29–67

Stöcklin J (1968) Structural history and tectonics of Iran: a review. AAPG Bull 52: 1229–1258

Taghizadeh-Farahmand F, Sodoudi F, Afsari N, Ghassemi MR (2010) Lithospheric structure of NW Iran from P and S receiver functions. J Seismol 14:823- 836

Tatar M, Jackson J, Hatzfeld D, Bergman E (2007) The 2004 May 28 Baladeh earthquake (mw 6,2) in the Alborz Iran: overthrusting the South Caspian Basin margin partitioning of oblique convergence and the seismic hazard of Tehran. Geophys J Int 170:249-261

Vernant P, Nilforoushan F, Hatzfeld D, Abassi MR, Vigny C, Masson F, Nankali H, Martinod J, Ashtiani A, Bayer R, Tavakoli F, Chéry J (2004) Present-day crustal deformation and plate kinematics in the Middle East constrained by GPS measurements in Iran and northern Oman. Geophys J Int 157: 381-398

Van de Zedde DMA, Wortel MJR (2001) Shallow slab detachment as a transient source of heat at midlithospheric depths. Tectonics 20 (6): 868-882

Vinnik LP (1977) Detection of waves converted from P to SV in the mantle. Physics of the Earth and Planetary Interiors 15: 39–45

Vinnik LP, Farra V, Kind R (2004) Deep structure of the Afro-Arabian hot spot by S receiver function. Geophys Res Lett 31:L11608

Vinnik LP, Reigber C, Aleshin IM, Kosarev GL, Kaban MK, Oreshin SI Roecker S (2004) Receiver function tomography of the central Tien Shan. Earth Planet. Sci. Lett 225: 131 – 146

Wong A, Ton SYM, Wortel MJR (1997) Slab detachment in continental collision zones: an analysis of controlling parameters. Geophys Res Lett 24: 2095-2098

Wortel MJR, Spakman W (2000) Subduction and slab detachment in the Mediterranean-Carpathian region. Science 290: 1910-1917.

Yuan X, Kind R, Li X, Wang R (2006) The S receiver functions: synthetics and data example. Geophys J Int 165(2): 555-564.

Yuan X, Ni J, Kind R, Mechie J, Sandvol E (1997) Lithospheric and upper mantle structure of southern Tibet from a seismological passive source experiment. J Geophys Res 102 (27): 491-500

Figure Captions

Figure 1. Main structural units in Iran.

Figure 2. Location map of 9 seismological stations (black stars) used in this study. Main tectonic units shown in Fig. 1 are illustrated with black dash lines. Distribution of the P-to-S (at 50 km) and S-to-P (at 100 km) conversions are indicated with white and blue crosses, respectively. Orange line marks the location of the profile used for Figs. 7 & 8. CD: Central Domain; UDMA: Urumieh-Dokhtar Magmatic Arc; SSZ: Sanandaj-Sirjan Zone; CIP: Central Iranian Plateau; ZFTB: Zagros Fold and Thrust Belt; MZT: Main Zagros Thrust.

Figure 3. Distribution of the teleseismic events recorded by the IIEES stations between 2006 to 2010 and used in this study. The center of the study area is shown by yellow star. The black and green solid circles indicate the 30°-90° (used for P receiver functions) and 60°-85° (used for S receiver functions) epicentral distances, respectively.

Figure 4. Individual P receiver functions for stations THKV and SNGE located in the Alborz zone and SSZ, respectively. Positive amplitudes are plotted in black, and negative amplitudes are shown in gray. Individual seismograms are plotted equally spaced and sorted according to their back azimuth. The P-to-S conversion from the Moho is labeled (M) on the summation traces.

Figure 5. Individual P receiver functions are stacked in bins of 0.05° and sorted by the latitude of their piercing points at 50 km depth for each tectonic zone. The P-to-S converted phase from the Moho is indicated by red dashed line. The arrival time of this phase varies between 5 and 8 s. The thickest crust is seen beneath the SSZ at 70 km (~ 8 s). **a)** Alborz zone **b)** ZFTB zone **c)** UDMA zone **d)** SSZ.

Figure 6. Individual S receiver functions sorted by the latitude of their piercing points at 100 km depth and shown for Alborz and ZFTB tectonic zones. Two phases are apparent in the data and are labeled Moho (red) and LAB (blue). **a)** Alborz zone **b)** ZFTB.

Figure 7. Migrated PRFs (upper panel) and SRFs (lower panel) along the SW-NE profile AA' shown in Fig. 2. The upper section shows the topography along the profile. Positive (negative) phases are shown in red (blue). PRFs section clearly shows the Moho boundary (dashed line) at depths ranging between 40-70 km. The thickest crust (70 km) is identified beneath the SSZ. Long periods SRFs resolve the Moho boundary at similar depths as observed in PRF data.

Figure 8. Stacked S receiver functions obtained from different tectonic zones along the SW-NE trending profile shown in Fig. 2. The upper section shows the topography along the profile. The arrival times of the Moho and LAB conversions are marked by white and black lines, respectively. The name of each tectonic zone is shown above each stacked trace. The Arabian LAB can be seen at 130 km depth beneath the ZFTB deepening to about 150 km beneath the SSZ, whereas the Central Iranian LAB is shallow and lies at 80-85 km depth.

Tables

Table 1. Station codes, station names, geographical coordinates, number of events used for PRF and SRF analysis in this study.

Table 2. The P-to-S and S-to-P conversion times (s) from the Moho, S-to-P conversion times (s) from the LAB and their corresponding depth (km) for different tectonic units used in this study.

Fig.1


Caspian Sea
Eurasian plate
Kopeh Dagh
Alborz Zone
Central Domain
Urumieh–Dokhtar Magmatic Arc
Sanandaj–Sirjan Zone
Main Zagros Thrust
Zagros Fold and Thrust Belt
Central Iranian Plateau
Helmand Block
Persian Gulf
Arabian pate
Oman Sea
44°
46°
48°
50°
52°
54°
56°
58°
60°
62°
64°
40°
38°
36°
34°
32°
30°
28°
26°
24°

Fig. 2

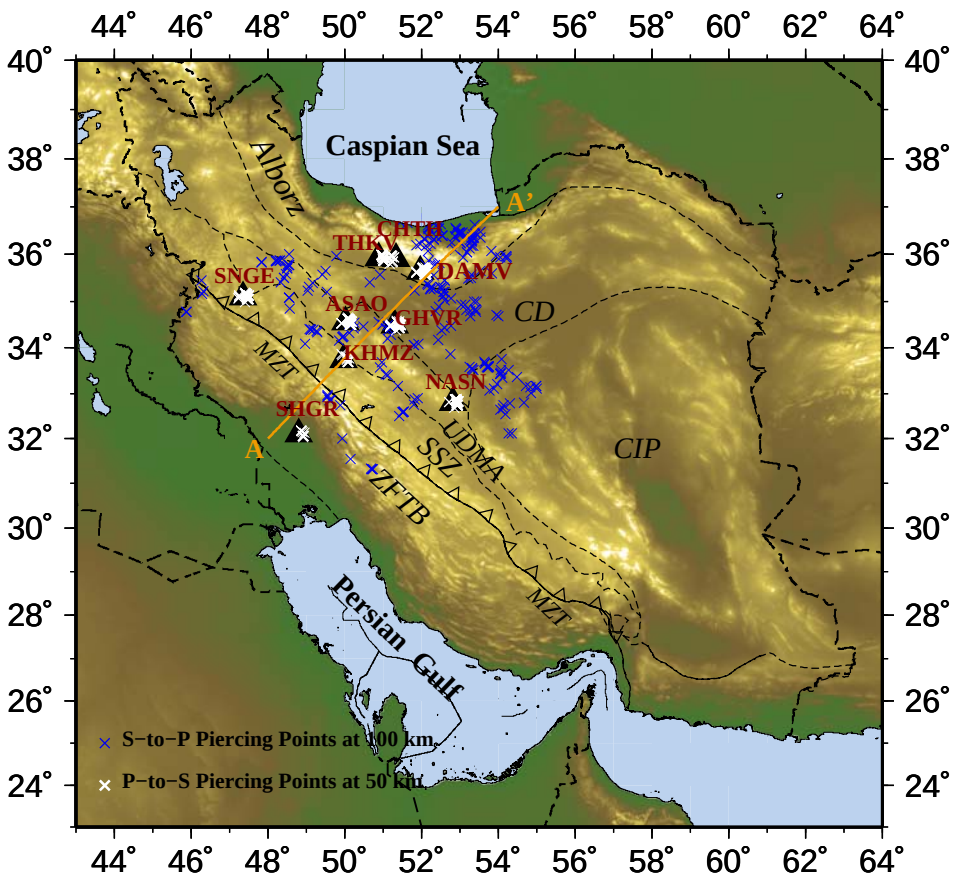
Caspian Sea
Alborz
A'
CHTH
THKV
DAMV
SNGE
ASAO
GHVR
CD
KHMZ
MZT
NASN
SHGR
A
UDMA
SSZ
ZFTB
CIP
Persian Gulf
MZT
S−to−P Piercing Points at 100 km
P−to−S Piercing Points at 50 km
44°
46°
48°
50°
52°
54°
56°
58°
60°
62°
64°
40°
38°
36°
34°
32°
30°
28°
26°
24°

Fig. 3

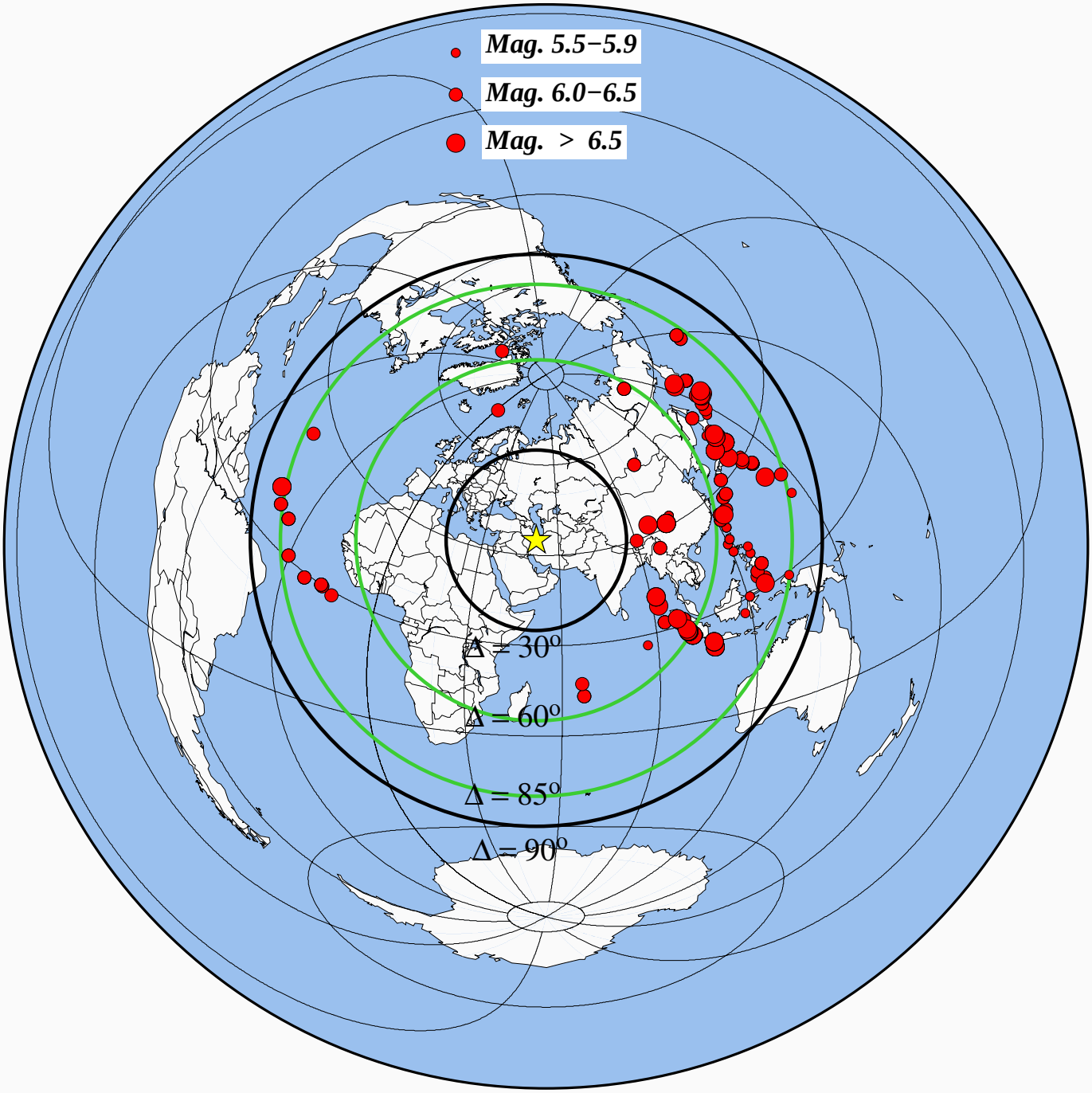

Fig. 4

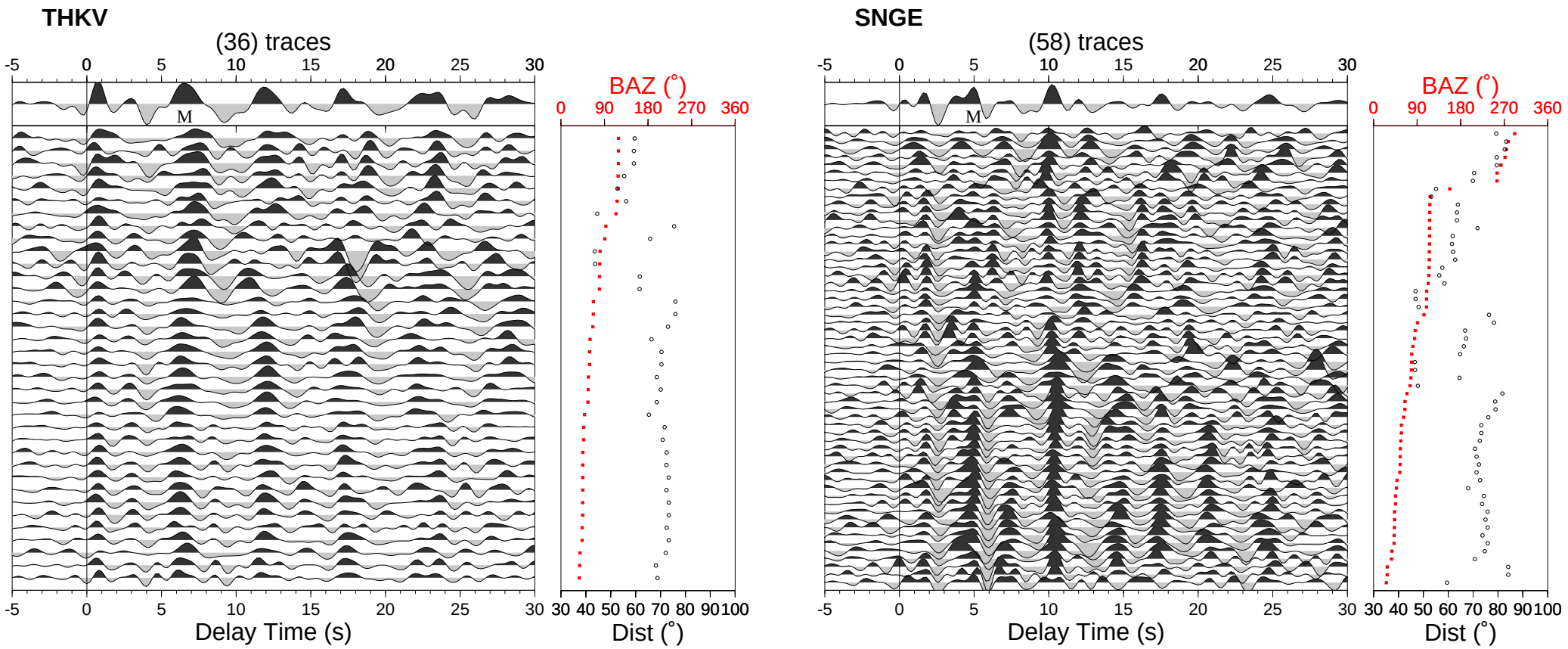
THKV
(36) traces
M
BAZ (°)
0 90 180 270 360
-5 0 5 10 15 20 25 30
30 40 50 60 70 80 90 100
Delay Time (s)
Dist (°)
SNGE
(58) traces
M
BAZ (°)
0 90 180 270 360
-5 0 5 10 15 20 25 30
30 40 50 60 70 80 90 100
Delay Time (s)
Dist (°)

Fig. 5

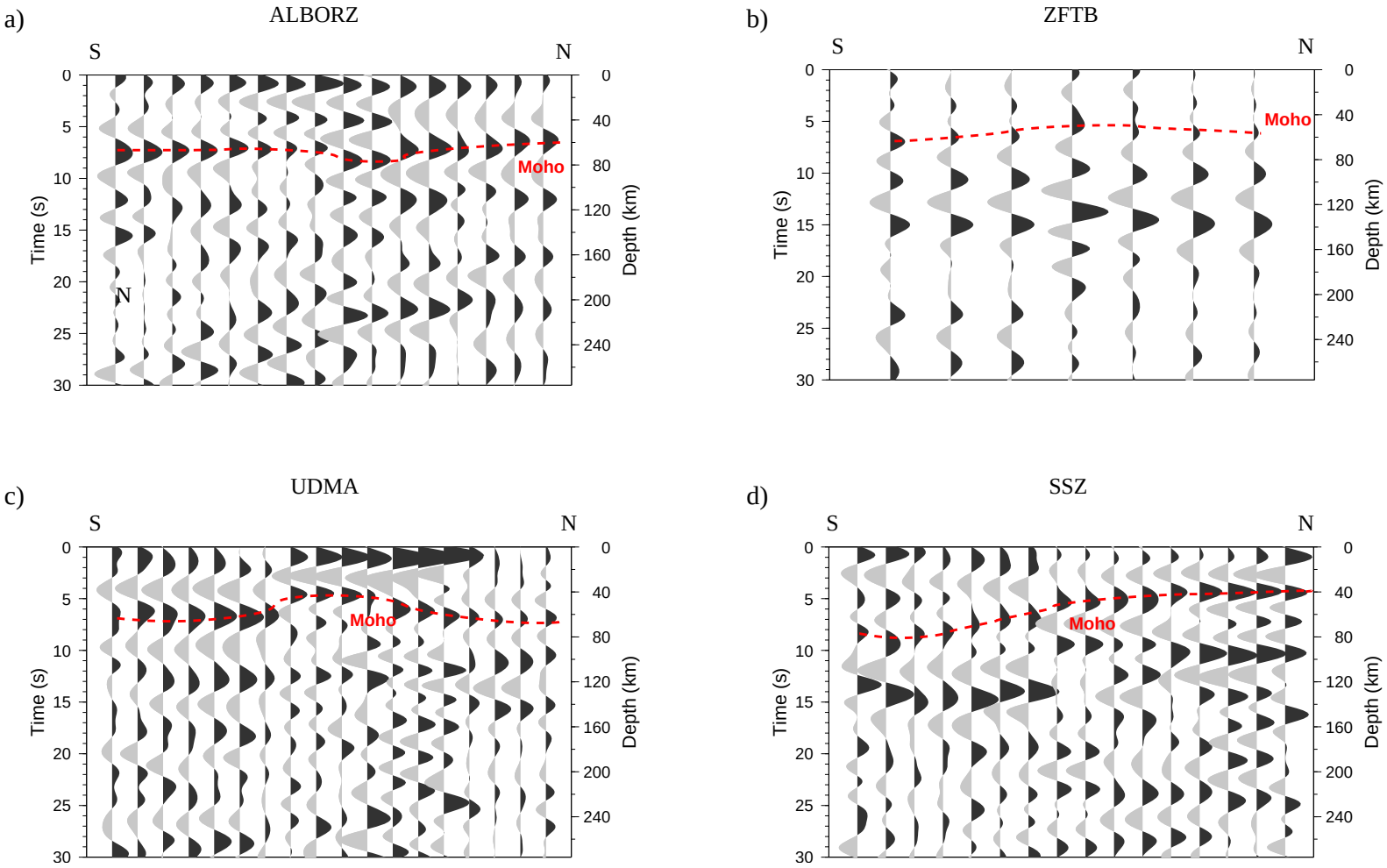
a)
ALBORZ
S
N
Moho
N
Time (s)
Depth (km)
b)
ZFTB
S
N
Moho
Time (s)
Depth (km)
c)
UDMA
S
N
Moho
Time (s)
Depth (km)
d)
SSZ
S
N
Moho
Time (s)
Depth (km)

Fig. 6

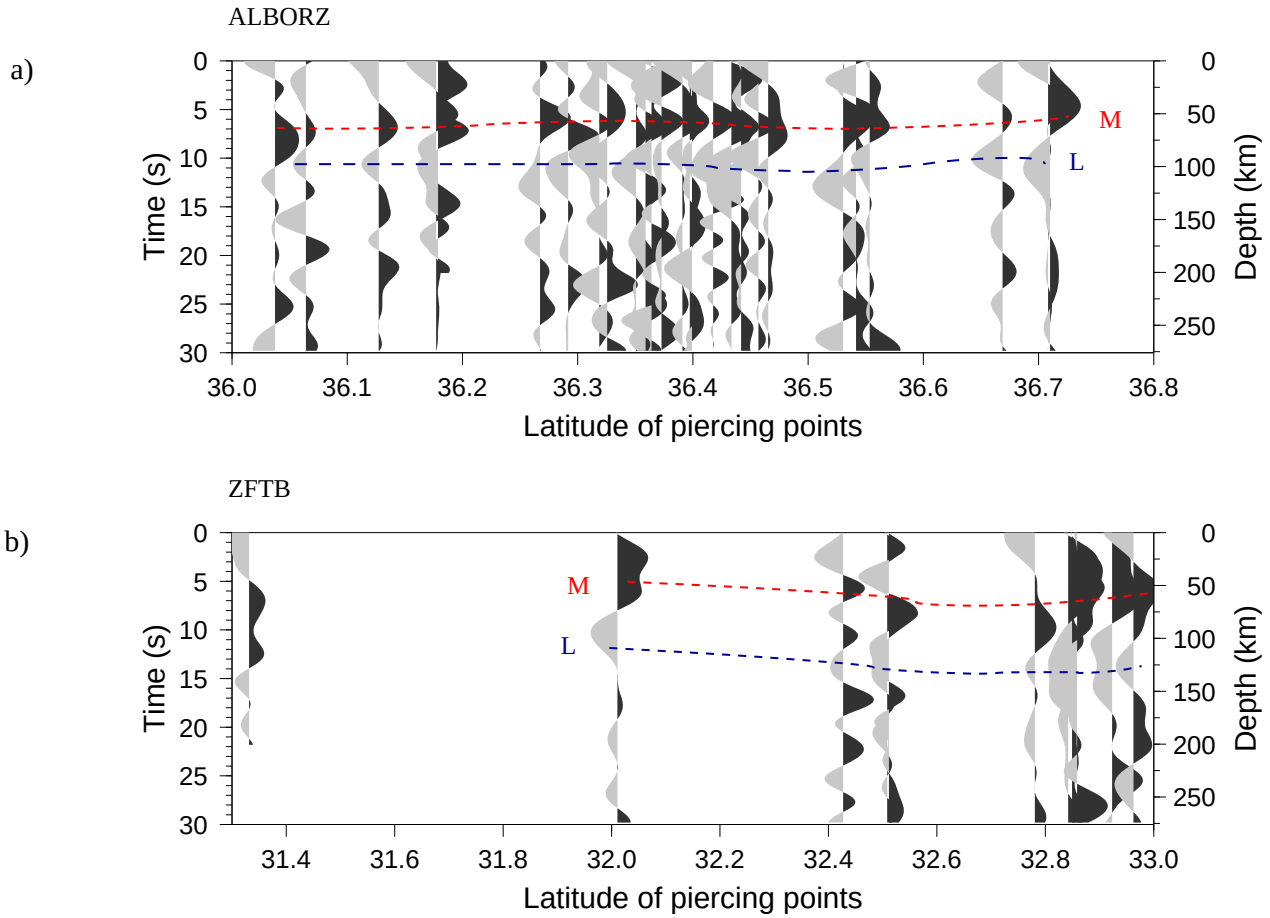
a)
ALBORZ
Time (s)
Depth (km)
M
L
Latitude of piercing points
b)
ZFTB
Time (s)
Depth (km)
M
L
Latitude of piercing points

Fig. 7

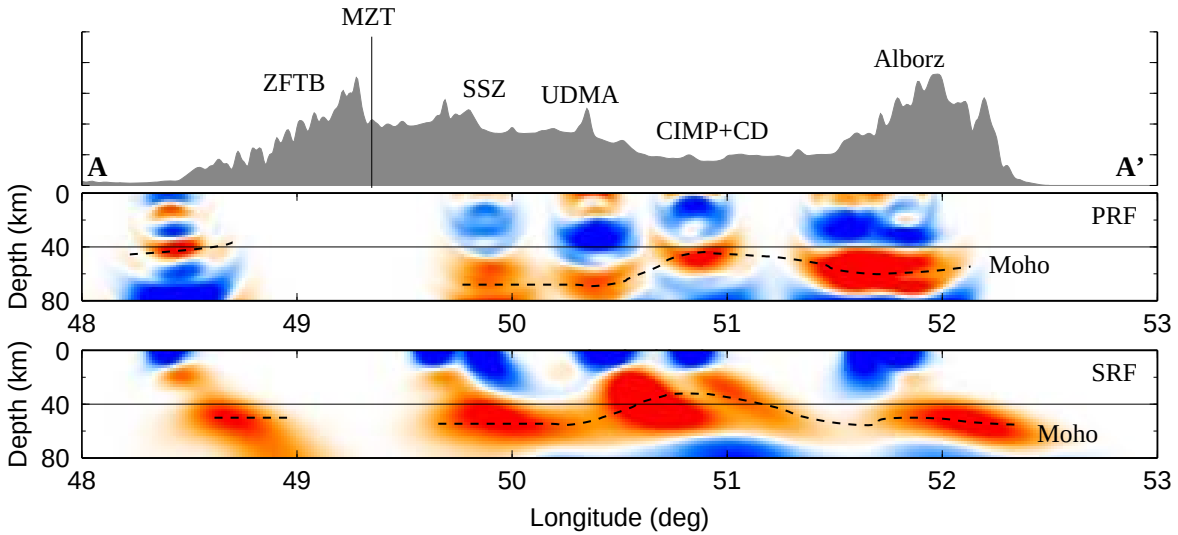
MZT
ZFTB
SSZ
UDMA
CIMP+CD
Alborz
A
A'
PRF
Moho
SRF
Moho
Depth (km)
0
40
80
48
49
50
51
52
53
Longitude (deg)

Fig. 8

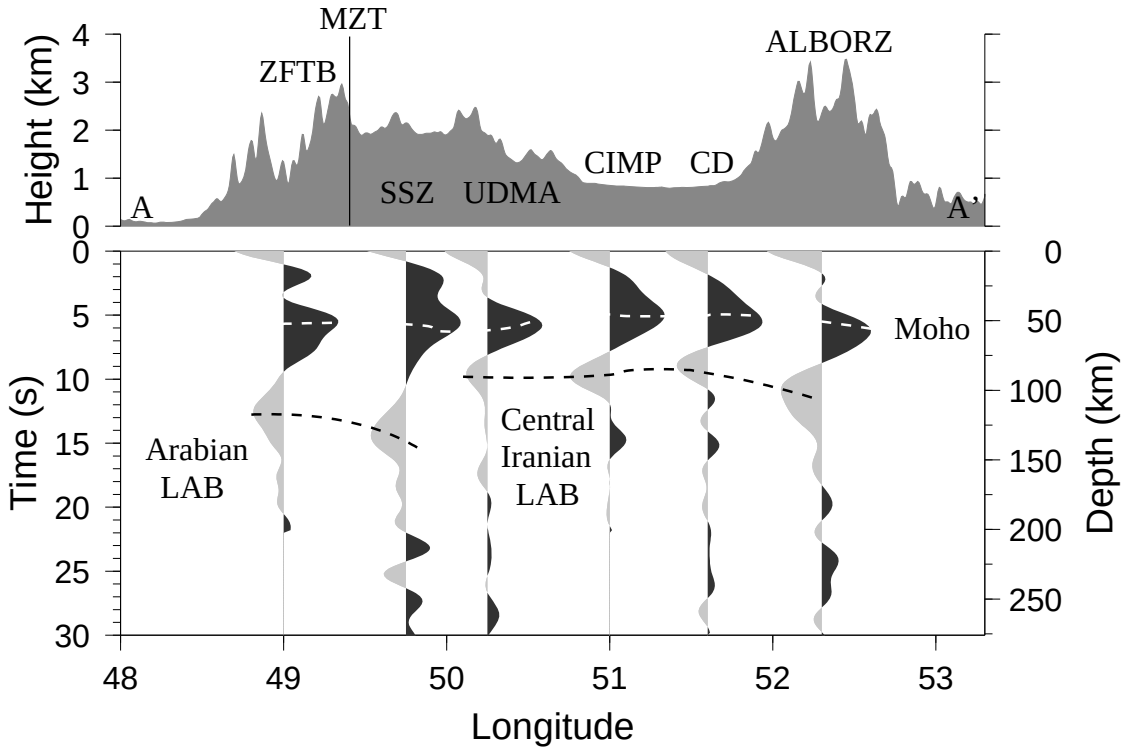
MZT
ZFTB
ALBORZ
CIMP
CD
SSZ
UDMA
A
A'
Height (km)
4
3
2
1
0
Moho
Arabian
LAB
Central
Iranian
LAB
Time (s)
0
5
10
15
20
25
30
Depth (km)
0
50
100
150
200
250
48
49
50
51
52
53
Longitude

Table 1. Station codes, station names, geographical coordinates, number of events used for PRF and SRF analysis in this study.

Station code	Station name	Longitude deg.	Latitude deg.	No. of PRFs	No. of SRFs
DAMV	Damavand	51.971	35.630	83	25
CHTH	Charan	51.126	35.908	13	11
THKV	Tehran	50.879	35.916	36	4
GHVR	Qom	51.295	34.480	37	12
ASAO	Ashtian	50.025	34.548	60	20
NASN	Naien	52.808	32.799	59	27
KHMZ	Khomein	49.959	33.739	17	5
SNGE	Sanandaj	47.347	35.093	58	15
SHGR	Shooshtar	48.801	32.108	16	11

Table 2. The P-to-S and S-to-P conversion times (s) from the Moho, S-to-P conversion times (s) from the LAB and their corresponding depth (km) for different tectonic units used in this study.

Studied zone	ZFT B	SSZ	UDMA	CD	CIP	Central Alborz
Moho conversion time (P-to-S)	6.0	5.0-8.0	5.0-7.0	-----	-----	6.5
Moho depth (km)	50	40-70	40-60	-----	-----	55
Moho conversion time (S-to-P)	6.0	6.0-8.0	6.0	5.0	4.5	6.5
Moho depth (km)	50	50-70	50	40	37	55
LAB conversion time (S-to-P)	13	15	9.5	9.0	9.5	10
LAB depth (km)	130	150	85	81	85	90